



## Bisulfite triggers fast oxidation of organic pollutants by colloidal MnO<sub>2</sub>

Bo Sun<sup>a,b,c,1</sup>, Zhongjin Xiao<sup>a,1</sup>, Hongyu Dong<sup>a</sup>, Shangchen Ma<sup>a</sup>, Guangfeng Wei<sup>d</sup>,  
Tongcheng Cao<sup>d</sup>, Xiaohong Guan<sup>a,e,\*</sup>

<sup>a</sup> State Key Laboratory of Pollution Control and Resources Reuse, Tongji University, Shanghai, 200092, China

<sup>b</sup> Department of Civil and Environmental Engineering, The Hong Kong University of Science and Technology, Clear Water Bay, Kowloon, Hong Kong, China

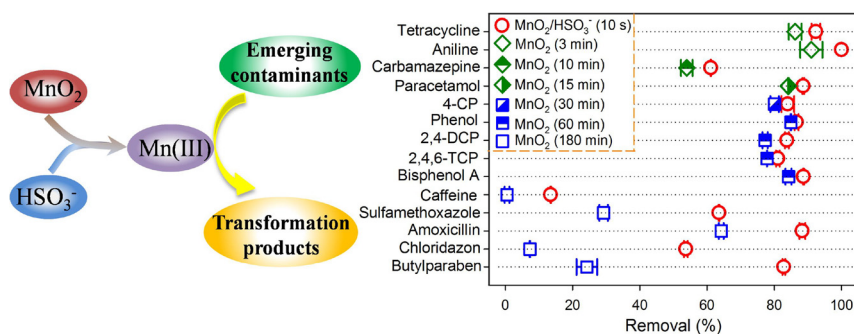
<sup>c</sup> Institute for Advanced Study, The Hong Kong University of Science and Technology, Hong Kong, China

<sup>d</sup> Shanghai Key Laboratory of Chemical Assessment and Sustainability, School of Chemical Science and Engineering, Tongji University, Shanghai, 200092, China

<sup>e</sup> Shanghai Institute of Pollution Control and Ecological Security, Shanghai, 200092, China



### GRAPHICAL ABSTRACT



### ARTICLE INFO

#### Keywords:

Advanced oxidation  
Manganese dioxide  
Bisulfite  
Mn(III)<sub>aq</sub>  
Electrophilic attack

### ABSTRACT

Colloidal MnO<sub>2</sub> is the most reactive phase of Mn(IV) while HSO<sub>3</sub><sup>-</sup> is a common reductant in water treatment. This study shows that the presence of HSO<sub>3</sub><sup>-</sup> resulted in significant increase in the decomposition rate of organic contaminants by colloidal MnO<sub>2</sub>. The degradation rate of contaminants in the MnO<sub>2</sub>/HSO<sub>3</sub><sup>-</sup> process dropped with elevating pH and a proper MnO<sub>2</sub>/HSO<sub>3</sub><sup>-</sup> molar ratio was critical for efficient decomposition of contaminants. The time-resolved spectroscopy of manganese species, the influence of pyrophosphate on UV absorbance spectra, and the relative rate constants of contaminants oxidation in MnO<sub>2</sub>/HSO<sub>3</sub><sup>-</sup> process suggested that the synergetic effect of HSO<sub>3</sub><sup>-</sup> and colloidal MnO<sub>2</sub> arose from the generation of Mn(III)<sub>aq</sub>, which could oxidize contaminants rapidly. The presence of pyrophosphate, ethylenediaminetetraacetic acid, and humic acid depressed the degradation of contaminants in MnO<sub>2</sub>/HSO<sub>3</sub><sup>-</sup> process by complexing with Mn(III)<sub>aq</sub>, buffering the solution or competing with contaminants for Mn(III)<sub>aq</sub>, and/or inhibiting the consumption of bisulfite. However, Ca<sup>2+</sup> and Mg<sup>2+</sup> accelerated the oxidation of contaminants in MnO<sub>2</sub>/HSO<sub>3</sub><sup>-</sup> process by enhancing the reduction of MnO<sub>2</sub> by HSO<sub>3</sub><sup>-</sup>. The good negative correlation of the O/N or H Mulliken charges of organic contaminants with their removal in MnO<sub>2</sub>/HSO<sub>3</sub><sup>-</sup> process suggested that organic contaminants were oxidized by Mn(III)<sub>aq</sub> via electrophilic attack.

\* Corresponding author at: State Key Laboratory of Pollution Control and Resources Reuse, Tongji University, Shanghai, 200092, China.

E-mail address: [guanxh@tongji.edu.cn](mailto:guanxh@tongji.edu.cn) (X. Guan).

<sup>1</sup> These authors contributed equally to this work.

## 1. Introduction

Manganese (Mn), a trace but essential element for life, is the second most abundant redox active transition metals in Earth's crust [1]. In environmental system, Mn exists mainly in three oxidation states: Mn(II), Mn(III), and Mn(IV) [2]. Electron transfers between Mn oxidation states are closely linked with other elemental cycles [3–7]. Mn oxides are thought to be the strongest, naturally occurring oxidants and are capable of transforming a wide range of organic substrates [8]. Besides the naturally occurring Mn oxides in a wide range of environmental setting, a wide variety of Mn oxides have also been employed to oxidize organic contaminants in water treatment. Compared to traditional advanced oxidation processes, Mn(III/IV) oxidation is demonstrated to be a convenient method to selectively degrade organic contaminants with electron-rich group [8]. It was reported that Mn(III) content and vacant sites in Mn oxide layers are rate controlling factors in the oxidation of contaminants [9,10]. Moreover, the reactivity of Mn oxides is closely related with their surface areas [8]. Therefore, colloidal MnO<sub>2</sub> is considered as the most reactive phase of Mn(IV) for contaminant abatement.

Although the utilization of Mn oxides as a polishing treatment step for contaminant removal is promising, the application of Mn oxides for contaminant oxidation faces several challenges [8]. First, Mn oxides are selective oxidants and Mn oxide-based reactors may have to be coupled with additional treatment processes to control other recalcitrant compounds. Second, the rates of organic contaminant oxidation by Mn oxides, including artificially synthesized colloidal MnO<sub>2</sub>, are highly variable, and moderate to slow for some contaminants [11–15]. Third, various conditions (e.g., pH and temperature) significantly influence the extent and kinetics of MnO<sub>2</sub> oxidation [16]. Co-existing solutes (e.g., metal ions, anions, and organic compounds) are thought to decrease the oxidizing power of MnO<sub>2</sub> by adsorption on, or competing with reactants for, reactive sites [17]. As a result, the application of MnO<sub>2</sub> is limited in water treatment. Thus, promoting the oxidation of organic contaminants by MnO<sub>2</sub> is becoming a necessity to achieve effective organic removal with MnO<sub>2</sub>. Xu et al. reported that humic acid could suppress the metal effect and substantially enhance organic removal, attributing to the complexation of humic acid with metal ions [15]. However, humic acid, as an organic compound, could influence the water quality and might lead to the generation of toxic by-products during disinfection process [18]. Sun et al. showed that the presence of pyrophosphate (PP) could promote the oxidation of phenol by MnO<sub>2</sub> under acidic conditions due to the generation of Mn(III)-PP complex, which serves as oxidant [19]. However, the concentration of PP should be several times higher than Mn concentration so as to generate stable Mn(III)-PP complex, which also results in secondary pollution. Recently, our preliminary study presented a delicious result that colloidal MnO<sub>2</sub> could be activated by HSO<sub>3</sub><sup>−</sup>, resulting in a process that oxidized organic contaminants at very high rates [20]. With the advantages of high oxidizing speed and the low cost of reagents, the MnO<sub>2</sub>/HSO<sub>3</sub><sup>−</sup> process has the potential to facilitate the practical application of MnO<sub>2</sub> in water treatment. To achieve this aim, it is imperative to clarify the detailed reaction mechanisms in MnO<sub>2</sub>/HSO<sub>3</sub><sup>−</sup> process and the influence of reaction conditions on the performance of this process.

Therefore, the present study was conducted to extensively explore the influence of HSO<sub>3</sub><sup>−</sup> on the redox activity of colloidal MnO<sub>2</sub>. Firstly, the kinetics of contaminant abatement by MnO<sub>2</sub>/HSO<sub>3</sub><sup>−</sup> were investigated as functions of pH and MnO<sub>2</sub>/HSO<sub>3</sub><sup>−</sup> molar ratio. To check the broad-spectrum of MnO<sub>2</sub>/HSO<sub>3</sub><sup>−</sup> process on degrading organic contaminants, the removal of a variety of emerging contaminants (ECs), which has caused great concerns in recent years [21–23], by MnO<sub>2</sub>/HSO<sub>3</sub><sup>−</sup> was compared with that by MnO<sub>2</sub> alone. Then, efforts were made to identify the active oxidant in the MnO<sub>2</sub>/HSO<sub>3</sub><sup>−</sup> process. Further, the influences of ligands and co-existing solutes on the performance of MnO<sub>2</sub>/HSO<sub>3</sub><sup>−</sup> process were illustrated. Finally, theoretical calculations were performed and the oxidation products of a selected

EC (sulfamethoxazole, SMX) were detected to clarify the mechanisms of organic decomposition in MnO<sub>2</sub>/HSO<sub>3</sub><sup>−</sup> process.

## 2. Materials and methods

### 2.1. Materials

A complete listing of reagents is provided in Supporting Information (SI) Text S1.

### 2.2. Stopped-flow experiments and batch experiments

The procedure of SFS experiments was described in our previous study [20]. The concentration of the target compound, methyl blue (MB), was determined by subtracting the absorbance of MnO<sub>2</sub> from the total absorbance at 626 nm examined with a UV-vis spectrophotometer. The absorbance of MnO<sub>2</sub> at 626 nm was obtained by timing that at 350 nm with the ratio of the molar absorptivity at 626 nm to that at 350 nm, since the absorption of MB at 350 nm could be neglected.

The details of batch experiments are presented in Text S2.

### 2.3. Chemical analysis

Ultra-performance liquid chromatography (UPLC) was employed to analyze the ECs and sodium ethylenediaminetetraacetic (EDTA). UPLC together with electrospray ionization quadrupole time-of-flight mass spectrometry (UPLC-QTOFMS) was used to detect the oxidation products of SMX. In this study, the mass spectrometer was operated in the *m/z* 50–1000 range and other details are presented in Text S3 of the Supporting Information. The concentration of residual bisulfite in MnO<sub>2</sub>/HSO<sub>3</sub><sup>−</sup> process was determined using a modified colorimetric procedure reported by Humphrey et al. with 5,5-dithiobis (2-nitrobenzoic acid) (DTNB) [24]. A detailed description of other analytical methods is provided in Text S4.

### 2.4. Methodology of theoretical calculations

The Gaussian package (versions G09 rev. D.01) at the density functional theory (DFT) level using B3LYP functional was employed to perform theoretical calculations. The influence of the solvent environment was modeled using the polarizable continuum solvent model (PCM) with parameters for water in cases of aqueous solutions [25]. Geometries of contaminants were optimized at the B3LYP/6-31+G(d,p) level of theory. Mulliken population analysis [26] was performed to gain the Mulliken charges on the nitrogen, oxygen, and hydrogen atoms of contaminants.

## 3. Results and discussion

### 3.1. Fast degradation of organic contaminants

The degradation kinetic of MB by MnO<sub>2</sub>/HSO<sub>3</sub><sup>−</sup> was determined with SFS at pH<sub>ini</sub> 5.0 and the result is shown in Fig. 1A. Over 90% of MB was removed by MnO<sub>2</sub>/HSO<sub>3</sub><sup>−</sup> in 7 s. MnO<sub>2</sub> alone oxidized MB much more slowly, as shown by the inset in Fig. 1A, and there was no detectable reduction of MB by NaHSO<sub>3</sub> (not shown). The presence of HSO<sub>3</sub><sup>−</sup> shortened the half-lives of MB oxidation by MnO<sub>2</sub> from 1702 s to 3.5 s. To model the degradation kinetic of MB by MnO<sub>2</sub>/HSO<sub>3</sub><sup>−</sup>, we fitted the majority of the data to pseudo-first-order kinetic after excluding a few data points that suggested an initial lag phase (Fig. 1A). The kinetic of MB oxidation by MnO<sub>2</sub> alone exhibited no lag, so these data was fitted as pseudo-first-order initial rate. The obtained pseudo-first-order rate constants (*k*<sub>obs</sub>) are summarized in Table S2. The oxidation rate of MB by MnO<sub>2</sub> at pH<sub>ini</sub> 5.0 was increased by 683 times due to the presence of HSO<sub>3</sub><sup>−</sup>, indicating that the MnO<sub>2</sub>/HSO<sub>3</sub><sup>−</sup> process

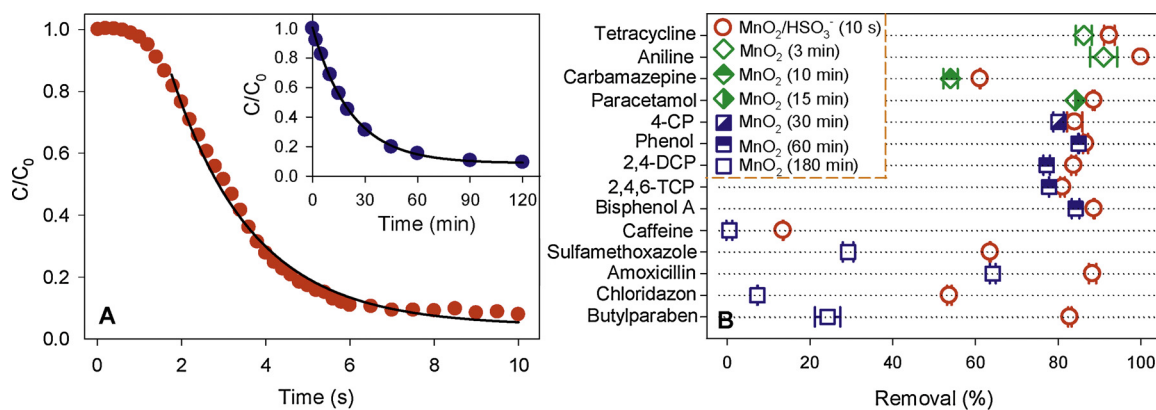


**Fig. 1.** Disappearance kinetics of MB (A) and the removal of selected emerging contaminants (B) by  $\text{MnO}_2/\text{HSO}_3^-$  and  $\text{MnO}_2$  alone. The inset of (A) was the degradation kinetic of MB by  $\text{MnO}_2$ . Reaction conditions:  $[\text{MnO}_2]_0 = 50 \mu\text{M}$ ,  $[\text{NaHSO}_3]_0 = 750 \mu\text{M}$ ,  $[\text{MB}]_0 = 3 \mu\text{M}$ ,  $[\text{test contaminants in Fig. 1(B)}]_0 = 5 \mu\text{M}$ ,  $\text{pH}_{\text{ini}} = 5.0$ ,  $T = 18 \pm 1^\circ\text{C}$ .

was an alternative method for rapid degradation of organic contaminants.

The influence of  $\text{pH}_{\text{ini}}$  on the degradation of MB by  $\text{MnO}_2/\text{HSO}_3^-$  and  $\text{MnO}_2$  alone was investigated. As shown in Fig. S1, the rate of MB degradation by  $\text{MnO}_2$  dropped considerably with increasing  $\text{pH}_{\text{ini}}$ . The dosing of  $\text{HSO}_3^-$  significantly accelerated the degradation of MB by  $\text{MnO}_2$  at various pH and the abatement rate of MB in  $\text{MnO}_2/\text{HSO}_3^-$  process decreased with elevating pH. The major portion of each data set of MB degradation kinetics by  $\text{MnO}_2/\text{HSO}_3^-$  and  $\text{MnO}_2$  alone can be well described by pseudo-first-order kinetics and the obtained pseudo-first-order rate constants at various pH levels are given in Table S2. Apparently, the presence of  $\text{HSO}_3^-$  enhanced the oxidation rate of MB by 91–683 times over the  $\text{pH}_{\text{ini}}$  range of 3.0–5.0. The decrease in the rate of MB degradation by  $\text{MnO}_2/\text{HSO}_3^-$  process with increasing pH should be mainly associated with the drop in the reduction rate of  $\text{MnO}_2$  by  $\text{HSO}_3^-$ , as demonstrated in Fig. S2A. Since the reduction of  $\text{MnO}_2$  to  $\text{Mn}^{2+}$  requires the participation of protons ( $\frac{1}{2}\text{MnO}_2 + 2\text{H}^+ + e^- \rightarrow \frac{1}{2}\text{Mn}^{2+} + \text{H}_2\text{O}$ ), the redox potential of  $\text{MnO}_2$  decreased from 0.876 V to 0.64 V with increasing pH from 3.0 to 5.0, which might account for the lower reactivity of  $\text{MnO}_2$  at higher pH [27]. There was a perfect correlation between the pseudo-first order rate constants of MB disappearance and those of  $\text{MnO}_2$  depletion at various  $\text{pH}_{\text{ini}}$  levels, as revealed by Fig. S2B, indicating the significant relationship between the consumption of  $\text{MnO}_2$  and the generation of reactive species responsible for contaminant oxidation.

The influence of  $\text{HSO}_3^-/\text{MnO}_2$  molar ratio on the degradation kinetics of MB by  $\text{MnO}_2/\text{HSO}_3^-$  process was also examined, as demonstrated in Fig. S3. With increasing the  $\text{HSO}_3^-/\text{MnO}_2$  molar ratio from 1 to 30, the rate of MB degradation increased progressively, which could be ascribed to both the larger reduction rate of  $\text{MnO}_2$  and the greater drop in pH with reaction at elevated  $\text{HSO}_3^-/\text{MnO}_2$  molar ratio, as shown in Fig. S4. However, the maximum removal efficiency of MB was achieved at  $\text{HSO}_3^-/\text{MnO}_2$  molar ratio of 15:1. Further increasing the initial concentration of  $\text{HSO}_3^-$  decreased the removal efficiency of MB, which might be ascribed to the consumption of active oxidant by excess  $\text{HSO}_3^-$ . There is an excellent correlation between  $\text{MnO}_2$  consumption and MB removal (Fig. S5) with  $\text{HSO}_3^-/\text{MnO}_2$  molar ratio of 1–15. In this study, the  $\text{HSO}_3^-/\text{MnO}_2$  molar ratio of 15:1 was employed in the following experiments unless otherwise noted.

ECs, including pharmaceuticals, personal care products, surfactants, industry additives, and endocrine disruptors, are a group of synthetic compounds which have recently detected at trace amounts in environment due to human activities [23,28]. Here, the abatement of 14 ECs with diverse organic moieties (as summarized in Table S1) in the  $\text{MnO}_2/\text{HSO}_3^-$  process was determined in 10 s, as illustrated in Fig. 1B. Considerable removal of butylparaben (82.8%), chloridazon (53.7%), amoxicillin (88.3%), SMX (63.6%), caffeine (13.5%), bisphenol A

(88.7%), 2,4,6-trichlorophenol (2,4,6-TCP, 81.1%), 2,4-dichlorophenol (2,4-DCP, 83.8%), phenol (86.6%), 4-chlorophenol (4-CP, 84.0%), paracetamol (88.6%), carbamazepine (CBZ, 61.1%), aniline (100%), tetracycline (92.4%) in the  $\text{MnO}_2/\text{HSO}_3^-$  process was observed in 10 s. Although the degradation experiments of these ECs by  $\text{MnO}_2$  alone lasted for 3–180 min, their extents of degradation were always less than those in the  $\text{MnO}_2/\text{HSO}_3^-$  process in 10 s. The discrepancy in the performance of these two methods was greater for butylparaben, chloridazon, amoxicillin, SMX, and caffeine than for other selected ECs since these five organic contaminants are much more recalcitrant than other selected ECs, suggesting that the  $\text{MnO}_2/\text{HSO}_3^-$  process is effective for removing various organic contaminants under acidic conditions.

### 3.2. The reactions involved in the $\text{MnO}_2/\text{HSO}_3^-$ process

As suggested in our previous study [20],  $\text{KMnO}_4$  can be activated by bisulfite, which denotes an equilibrium mixture of  $\text{HSO}_3^-$  and  $\text{SO}_3^{2-}$ , to generate aquo Mn(III) ( $\text{Mn(III)}_{\text{aq}}$ , noncomplexed with ligands other than  $\text{H}_2\text{O}$  and  $\text{OH}^-$ ).  $\text{Mn(III)}_{\text{aq}}$  oxidizes organic contaminants at very high rates [29]. The analogous effects of bisulfite on the oxidation of organic contaminants by  $\text{KMnO}_4$  and  $\text{MnO}_2$  as well as the correlation of  $\text{MnO}_2$  reduction with contaminant oxidation (Fig. S2B and S5) suggest that  $\text{Mn(III)}_{\text{aq}}$  may also be responsible for the enhanced organic contaminant abatement in the  $\text{MnO}_2/\text{HSO}_3^-$  process. Recently,  $\text{HO}^\bullet$  and/or  $\text{SO}_4^{\cdot-}$  were identified to be the reactive oxidants account for the oxidation of organic contaminants in several sulfite involved oxidation processes, including  $\text{Cr(VI)}/\text{SO}_3^{2-}$  process [30],  $\text{Fe(VI)}/\text{SO}_3^{2-}$  process [31],  $\text{Mn}^{2+}/\text{SO}_3^{2-}$  [32], and  $\text{Fe}^{2+}/\text{SO}_3^{2-}$  process [33]. However, the contribution of  $\text{HO}^\bullet$  and  $\text{SO}_4^{\cdot-}$  as major oxidants in  $\text{KMnO}_4/\text{HSO}_3^-$  has been excluded in our previous study with electron spin resonance (ESR) experiments [20]. In this study, relative rate method was employed to further negate the possibility of  $\text{HO}^\bullet$  and  $\text{SO}_4^{\cdot-}$  as the major active species in the  $\text{MnO}_2/\text{HSO}_3^-$  process so as to support the contribution of  $\text{Mn(III)}_{\text{aq}}$  in this process. As shown in Fig. 2, the second order rate constants of benzoic acid (BA) oxidation are 11.1 and 3.7 times lower than phenol and CBZ oxidation, respectively, in the  $\text{MnO}_2/\text{HSO}_3^-$  process. However, the relative rate of BA and phenol oxidation ( $k_{\text{BA}}/k_{\text{Phenol}}$ ) should vary from 0.89 to 0.14 and the relative rate of BA and CBZ oxidation ( $k_{\text{BA}}/k_{\text{CBZ}}$ ) would vary from 0.59 to 0.77 if  $\text{HO}^\bullet$  and/or  $\text{SO}_4^{\cdot-}$  are the main reactive species [34–38]. Therefore, the reactivity of active oxidant in  $\text{MnO}_2/\text{HSO}_3^-$  process is quite different from that of  $\text{HO}^\bullet$  and  $\text{SO}_4^{\cdot-}$  towards different organic contaminants, indicating that the active oxidant in  $\text{MnO}_2/\text{HSO}_3^-$  process is different from  $\text{HO}^\bullet$  or  $\text{SO}_4^{\cdot-}$ . In addition, the involvement of  $\text{HO}^\bullet$  or  $\text{SO}_4^{\cdot-}$  in  $\text{MnO}_2/\text{HSO}_3^-$  process was further excluded by determining the generation of formaldehyde in the presence of excess alcohols. Many studies showed that  $\text{HO}^\bullet$  and  $\text{SO}_4^{\cdot-}$

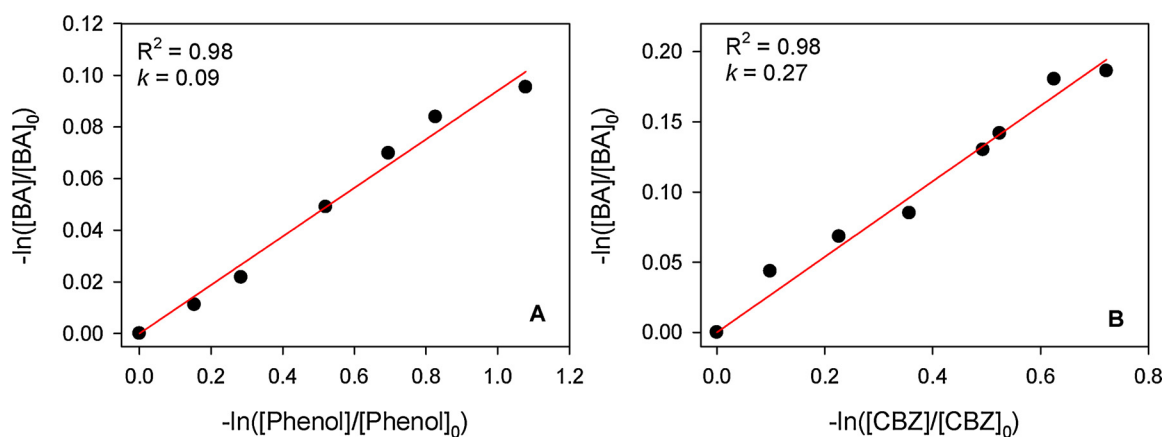


Fig. 2. Relative rates of (A) phenol and BA oxidation, (B) BA and CBZ oxidation in the  $\text{MnO}_2/\text{HSO}_3^-$  process. Reaction conditions:  $[\text{Phenol}]_0 = 20 \mu\text{M}$ ,  $[\text{BA}]_0 = 10 \mu\text{M}$ ,  $[\text{CBZ}]_0 = 20 \mu\text{M}$ ,  $[\text{MnO}_2]_0 = 0\text{--}100 \mu\text{M}$ , the molar ratio of  $\text{NaHSO}_3$  to  $\text{MnO}_2$  is fixed at 15,  $\text{pH}_{\text{ini}} = 5.0$ ,  $T = 18 \pm 1^\circ\text{C}$ .

could oxidize alcohols to formaldehyde [39–41]. However, no formaldehyde was detected during the reaction ( $[\text{MnO}_2]_0 = 50 \mu\text{M}$ ,  $[\text{HSO}_3^-]_0 = 250 \mu\text{M}$ ,  $[\text{tert-butyl alcohol}]_0 = 250 \text{ mM}$ ,  $\text{pH}_{\text{ini}} = 5.0$ ), suggesting the negligible contribution of  $\text{HO}^\cdot$  and  $\text{SO}_4^{\cdot-}$  to contaminant degradation in the  $\text{MnO}_2/\text{HSO}_3^-$  process. The generation of  $\text{HO}^\cdot$  or  $\text{SO}_4^{\cdot-}$  in the  $\text{Mn}^{2+}/\text{HSO}_3^-$  system at  $\text{pH}_{\text{ini}} 5.0$  was also excluded since no SMX was degraded in the  $\text{Mn}^{2+}/\text{HSO}_3^-$  system accompanied with the  $\text{HSO}_3^-$  consumption, as shown in Fig. S6. The possibility of  $\text{SO}_5^{\cdot-}$  as the major reactive species for contaminant oxidation in  $\text{MnO}_2/\text{HSO}_3^-$  process was excluded by analyzing the effect of 1-hexanol on atrazine oxidation [42]. The second-order rate constants of contaminant oxidation by  $\text{SO}_5^{\cdot-}$  are usually in the range of  $10^5\text{--}10^7 \text{ M}^{-1}\text{s}^{-1}$ , whereas the rate constant of  $\text{SO}_5^{\cdot-}$  towards 1-hexanol is less than  $10^3 \text{ M}^{-1}\text{s}^{-1}$  [42]. Therefore, the removal of  $5 \mu\text{M}$  atrazine in the  $\text{MnO}_2/\text{HSO}_3^-$  process should not be less than 20% in the presence of  $2 \text{ mM}$  1-hexanol, as described in Eq. (1). However, as shown in Fig. S7, only 12% of atrazine was removed in the presence of  $2 \text{ mM}$  1-hexanol, which proved that the  $\text{SO}_5^{\cdot-}$  was not the major reactive species for contaminant oxidation in  $\text{MnO}_2/\text{HSO}_3^-$  process.

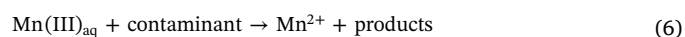
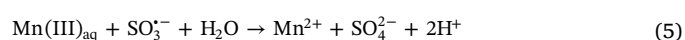
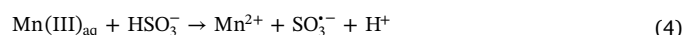
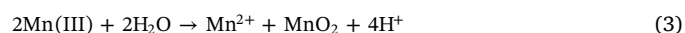
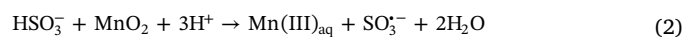
$$\frac{k_{\text{atrazine}}}{k_{1\text{-hexanol}}} > \frac{10^5 \text{ M}^{-1}\text{s}^{-1} \times 5 \times 10^{-6} \text{ M}}{10^3 \text{ M}^{-1}\text{s}^{-1} \times 2 \times 10^{-3} \text{ M}} = 0.2 \quad (1)$$

where  $k_{\text{atrazine}}$  and  $k_{1\text{-hexanol}}$  are the consumption rates of  $\text{SO}_5^{\cdot-}$  by atrazine and 1-hexanol, respectively.

It is well known that Mn(III) stabilized by complexation with PP has an absorbance peak at 258 nm and thus this characteristic absorbance was commonly used in the literatures for identifying the role of Mn(III) in various processes [7,43]. In this study, the time-resolved three-dimensional UV-vis spectra for the reaction of  $\text{MnO}_2$  with  $\text{HSO}_3^-$  with and without PP were collected with SFS to further clarify the contribution of  $\text{Mn(III)}_{\text{aq}}$  in  $\text{MnO}_2/\text{HSO}_3^-$  process. As shown in Fig. 3A, the spectrum of  $\text{MnO}_2$  was dominant at the beginning. In the absence of PP,  $\text{MnO}_2$  was reduced to  $\text{Mn}^{2+}$  gradually and there was no obvious absorbance at 230–350 nm at the end of reaction. In the presence of PP (Fig. 3B), a broad peak appearing at  $\sim 260 \text{ nm}$  was observed, indicating the possible formation of Mn(III)-PP. As PP might change the balance of manganese species and induce the generation of Mn(III)-PP, methanol was added to the  $\text{MnO}_2/\text{HSO}_3^-/\text{PP}$  mixture to clarify the contribution of  $\text{Mn(III)}_{\text{aq}}$  in this process. It should be noted that the reactivity of Mn(III)-PP towards organics is much lower than uncomplexed  $\text{Mn(III)}_{\text{aq}}$  [20]. As shown in Fig. 3C, in the presence of both PP and methanol, the absorbance arising from Mn(III)-PP is negligible. The above evidences confirming that: (1)  $\text{Mn(III)}_{\text{aq}}$  generated in the  $\text{MnO}_2/\text{HSO}_3^-$  process oxidizes methanol at a greater rate than it complexes with PP, (2) the complexation of  $\text{Mn(III)}_{\text{aq}}$  with PP is faster than the disproportionation of  $\text{Mn(III)}_{\text{aq}}$ , (3) the generation of Mn(III)-PP in Fig. 3B should be ascribed to the complexation of *in situ* formed  $\text{Mn(III)}_{\text{aq}}$  with PP rather

than the comproportionation of Mn(II) with  $\text{MnO}_2$  in the presence of PP. To further clarify the generation of Mn(III)-PP, the UV-vis spectra over a wider wavelength were recorded after reduction of  $\text{MnO}_2$  by  $\text{HSO}_3^-$  with and without PP, as illustrated in Fig. S8. The spectra of colloidal  $\text{MnO}_2$  and synthesized Mn(III)-PP were also plotted in Fig. S8 for reference. The spectrum of the mixture of  $\text{MnO}_2$  and  $\text{HSO}_3^-$  showed predominantly the spectrum of residual  $\text{MnO}_2$  without PP (spectrum a in Fig. S8). In the presence of PP, the spectrum (spectrum b in Fig. S8) showed the characteristic peaks arising from both Mn(III)-PP and  $\text{MnO}_2$ . After subtracting the absorbance of  $\text{MnO}_2$  from spectrum b, a peak at 258 nm was left behind, which was characteristic of the absorbance of Mn(III)-PP, confirming the generation of  $\text{Mn(III)}_{\text{aq}}$  during the reduction of  $\text{MnO}_2$  by  $\text{HSO}_3^-$ . As the molar absorption coefficient of Mn(III)-PP at 258 nm is  $6750 \text{ M}^{-1}$  [43], the concentration of Mn(III)-PP was determined to be  $15.7 \mu\text{M}$ . Deducting the generated Mn(III)-PP and residual  $\text{MnO}_2$  ( $\sim 8 \mu\text{M}$ ) from dosed  $\text{MnO}_2$  ( $50 \mu\text{M}$ ),  $\sim 26.3 \mu\text{M}$  Mn(II) was produced, indicating that the amount of Mn(III) and/or Mn(III)-PP reduced by  $\text{HSO}_3^-/\text{SO}_3^{\cdot-}$  was  $\sim 26.3 \mu\text{M}$  within 60 s in this case [44].

Analogous to the reaction mechanisms involved in the process of organic contaminant degradation by  $\text{KMnO}_4/\text{HSO}_3^-$  [44], a simplified reaction scheme for contaminant oxidation in the  $\text{MnO}_2/\text{HSO}_3^-$  process was proposed, as illustrated in Eqs. (1)–(9). In this reaction scheme,  $\text{MnO}_2$  was reduced by  $\text{HSO}_3^-$  to form  $\text{Mn(III)}_{\text{aq}}$  (Eq. (2)).  $\text{Mn(III)}_{\text{aq}}$  was very unstable and would rapidly transform to  $\text{Mn}^{2+}$  by disproportionation (Eq. (3)) or reduction by  $\text{HSO}_3^-/\text{SO}_3^{\cdot-}$  (Eqs. (4) and (5)). When organic contaminants were present,  $\text{Mn(III)}_{\text{aq}}$  could be consumed by oxidizing organic contaminants (Eq. (6)). Since the reaction was carried out open to the air, the transformation of sulfur species in the presence of oxygen were proposed in Eqs. (7)–(10) [44].



According to the proposed reaction mechanisms, the degradation of organic contaminants by  $\text{MnO}_2/\text{HSO}_3^-$  was not favorable at either very

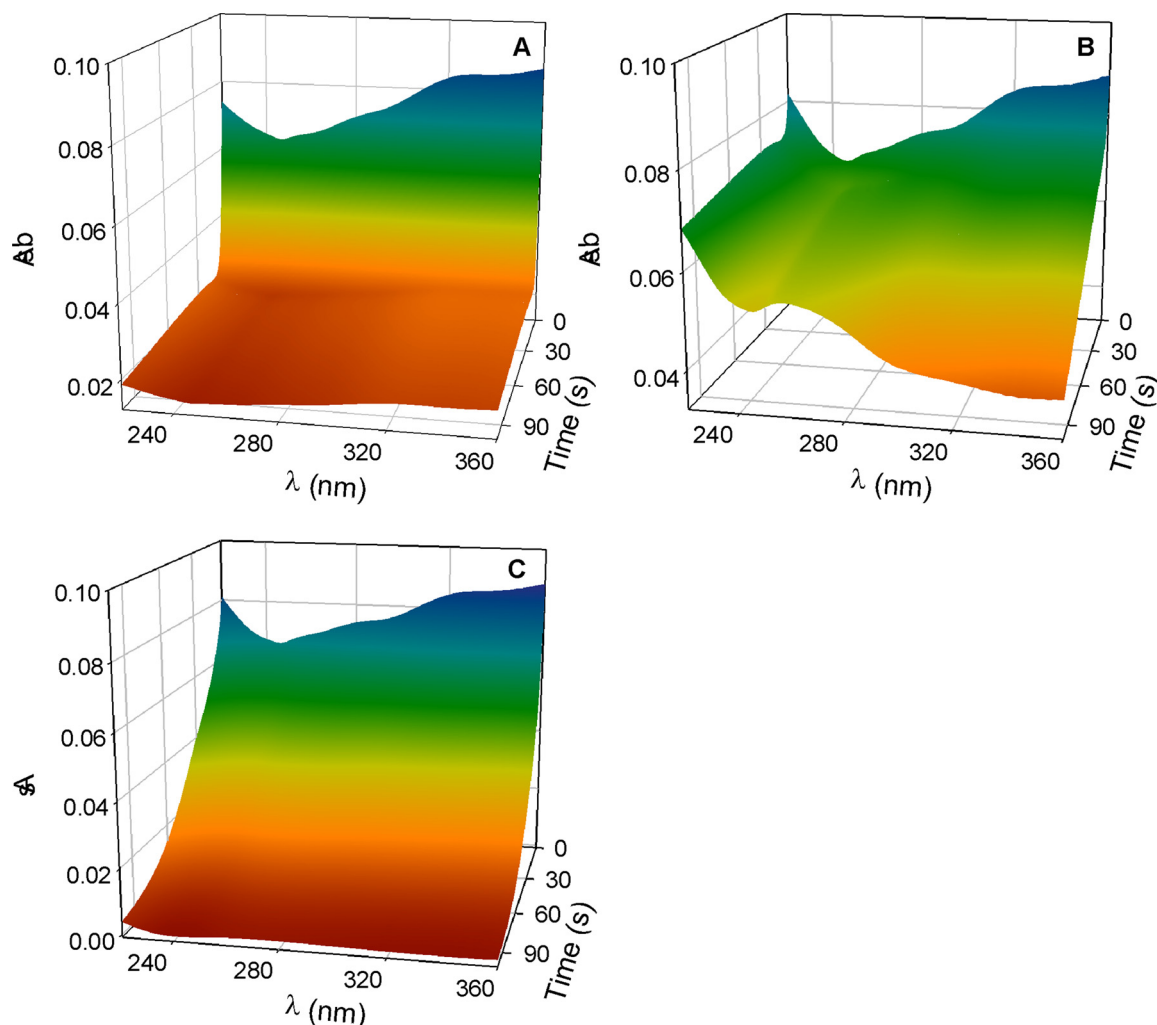


**Fig. 3.** Three-dimensional UV-vis spectra during the reaction of (A)  $\text{MnO}_2$  with  $\text{HSO}_3^-$ , (B)  $\text{MnO}_2$  with  $\text{HSO}_3^-$  in the presence of PP, (C)  $\text{MnO}_2$  with  $\text{HSO}_3^-$  in the presence of PP and methanol. Reaction conditions:  $[\text{MnO}_2]_0 = 50 \mu\text{M}$ ,  $[\text{NaHSO}_3]_0 = 750 \mu\text{M}$ ,  $[\text{PP}]_0 = 5 \text{ mM}$ ,  $[\text{Methanol}]_0 = 20 \text{ mM}$ ,  $\text{pH}_{\text{ini}} = 5.0$ ,  $T = 18 \pm 1^\circ\text{C}$ .

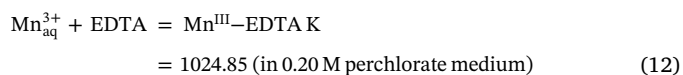
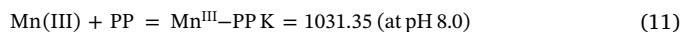
low  $\text{HSO}_3^-$  concentration or very high  $\text{HSO}_3^-$  concentration. At low  $\text{HSO}_3^-$  concentration, the generation of  $\text{Mn(III)}_{\text{aq}}$  was the limiting factor of organic contaminants abatement due to the consumption of  $\text{HSO}_3^-$  by oxygen. On the other hand, excessive  $\text{HSO}_3^-$  could consume the generated  $\text{Mn(III)}_{\text{aq}}$  and thus depressed the oxidation of organic contaminants by  $\text{Mn(III)}_{\text{aq}}$ , which was in agreement with the data presented in Fig. S3. The final pH in the process of organic contaminant degradation by  $\text{MnO}_2/\text{HSO}_3^-$  as functions of initial  $\text{HSO}_3^-$  concentration and initial concentration of organic contaminant (SMX was employed as an example), as demonstrated in Figs. S9 and S10, was also consistent with the proposed mechanisms. In brief, the increase in initial  $\text{HSO}_3^-$  concentration would result in a drop in pH arising from the release of protons due to the oxidation of  $\text{HSO}_3^-$  by oxygen (Eqs. (7)–(10)). However, the final pH elevated with increasing the initial SMX concentration since the presence of excess organic contaminant would inhibit the disproportionation of  $\text{Mn(III)}_{\text{aq}}$  (Eq. (3)) and the reduction of  $\text{Mn(III)}_{\text{aq}}$  by  $\text{HSO}_3^-/\text{SO}_3^{\cdot-}$  (Eqs. (4) and (5)) and thus decreased the amount of released protons. These experimental results and analysis further affirmed the validity of the proposed mechanisms.

### 3.3. Influence of ligands on the degradation kinetics of MB by $\text{MnO}_2/\text{HSO}_3^-$

Ligands could stabilize Mn(III) and reduce the reactivity of Mn(III) [7,45,46]. PP and EDTA, which are known to form strong complexes

with Mn(III), were chosen as typical ligands since PP was a non-redox active ligand while EDTA was an organic ligand associated with water contamination [47].

The four acidity constants pyrophosphoric acid are 1.5, 2.0, 6.8, and 8.7, respectively [48]. EDTA has six acidity constants and they are 0.0, 1.5, 2.0, 2.7, 6.1, and 10.2, respectively [49]. Thus, both ligands may play a role of buffer over a wide pH range. Moreover, the conditional stability constants for Mn(III) complexes reported in the literature were listed as follows [43,47],



The standard reduction potential,  $E_H^0$ , for the half reaction  $\text{Mn}_{\text{aq}}^{3+} + e^- = \text{Mn}_{\text{aq}}^{2+}$  is approximately 1.5 V [50]. However, the standard reduction potentials for Mn(III) in the presence of PP and EDTA were estimated to be 1.15 V and 0.824 V [47], respectively. Thus, it can be inferred that the reactivity of Mn(III) will drop greatly once it forms complex with either PP or EDTA.

With increasing the PP concentration from 10  $\mu\text{M}$  to 5000  $\mu\text{M}$ , the degradation rate of MB by  $\text{MnO}_2/\text{HSO}_3^-$  dropped progressively and the amount of degraded MB at equilibrium decreased, as shown in Fig. 4A. However, ~26% of MB could be decomposed by  $\text{MnO}_2/\text{HSO}_3^-$  even when the concentration of PP was as high as 5000  $\mu\text{M}$ , indicating that

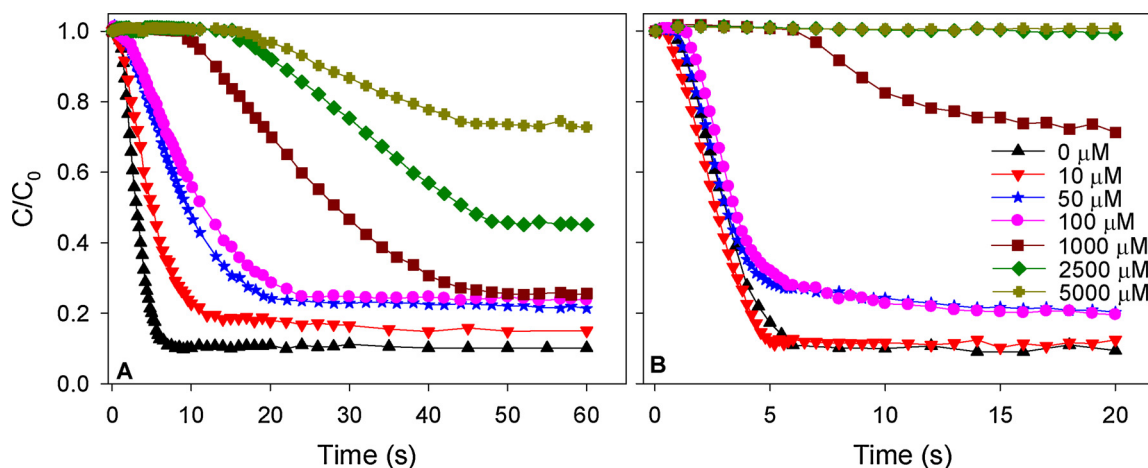


Fig. 4. Influence of PP (A) and EDTA (B) with different concentrations on the degradation kinetics of MB in the  $\text{MnO}_2/\text{HSO}_3^-$  system. Reaction conditions:  $[\text{MnO}_2]_0 = 50 \mu\text{M}$ ,  $[\text{NaHSO}_3]_0 = 750 \mu\text{M}$ ,  $[\text{MB}]_0 = 3 \mu\text{M}$ ,  $\text{pH}_{\text{ini}} = 5.0$ ,  $T = 18 \pm 1 \text{ }^\circ\text{C}$ .

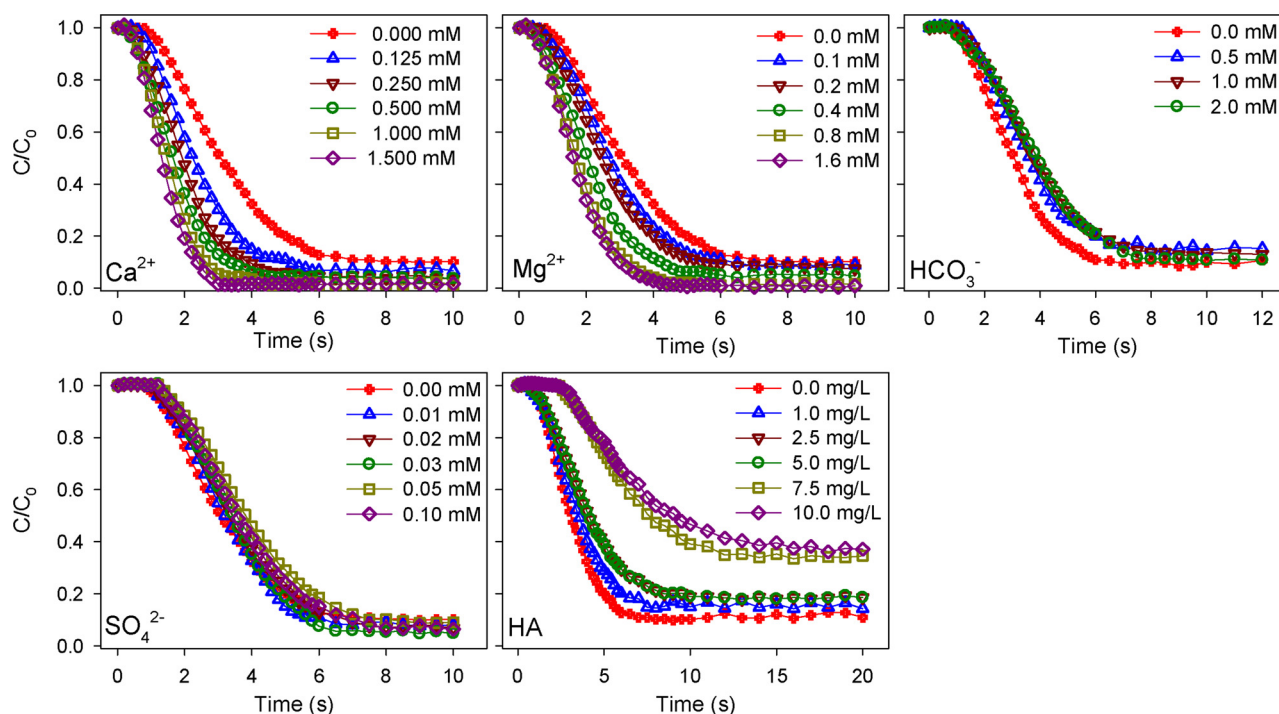


Fig. 5. Influence of co-existing substances of various concentrations on the degradation of MB in the  $\text{MnO}_2/\text{HSO}_3^-$  system. Reaction conditions:  $[\text{MnO}_2]_0 = 50 \mu\text{M}$ ,  $[\text{NaHSO}_3]_0 = 750 \mu\text{M}$ ,  $[\text{MB}]_0 = 3 \mu\text{M}$ ,  $\text{pH}_{\text{ini}} = 5.0$ ,  $T = 18 \pm 1 \text{ }^\circ\text{C}$ .

the complexation rate of  $\text{Mn(III)}_{\text{aq}}$  with PP was slower than the oxidation rate of MB by  $\text{Mn(III)}_{\text{aq}}$ . Otherwise, negligible MB could be oxidized at very high PP concentration since  $\text{Mn(III)-PP}$  had negligible reactivity compared to the uncomplexed  $\text{Mn(III)}_{\text{aq}}$ , as revealed by our previous study [20]. In addition, PP is a buffer and it can mediate the pH drop during organic contaminant oxidation by  $\text{MnO}_2/\text{HSO}_3^-$  (Fig. S11) and thus retard the reaction between  $\text{MnO}_2$  and  $\text{HSO}_3^-$  (Fig. S12A and S13A). Consequently, it would decrease the rate of  $\text{Mn(III)}_{\text{aq}}$  generation and organic contaminant decomposition. In sum, PP affected the process of organic contaminant oxidation by  $\text{MnO}_2/\text{HSO}_3^-$  primarily as a pH buffer and secondarily as complexing agent.

EDTA, a redox active ligand, had more complicated influence on MB removal by  $\text{MnO}_2/\text{HSO}_3^-$ , as illustrated in Fig. 4B. EDTA dosed at  $10 \mu\text{M}$  accelerated the oxidation of MB by  $\text{MnO}_2/\text{HSO}_3^-$ , which may be ascribed to the enhanced reduction of  $\text{MnO}_2$  by  $\text{HSO}_3^-$  and the improved generation of  $\text{Mn(III)}_{\text{aq}}$ . EDTA with concentration  $\geq 50 \mu\text{M}$  depressed the removal of MB by  $\text{MnO}_2/\text{HSO}_3^-$  and the removal of MB

was completely inhibited when the concentration of EDTA was increased to  $2500\text{--}5000 \mu\text{M}$ . However, EDTA with concentration  $\leq 100 \mu\text{M}$  accelerated  $\text{MnO}_2$  reduction and it decelerated  $\text{MnO}_2$  reduction only slightly when it was dosed at  $1000\text{--}5000 \mu\text{M}$  (Fig. S12B). The presence of  $50\text{--}5000 \mu\text{M}$  EDTA greatly decreased the consumption of bisulfite, as shown in Fig. S13B, implying that EDTA inhibited the oxidation of bisulfite by oxygen at elevated concentration of EDTA. Wang et al. [51] observed that ethanol inhibited the oxidation of sulfite by oxygen in water due to the interaction of ethanol with  $\text{SO}_3^{\cdot-}$ . Therefore, the decrease in bisulfite oxidation by oxygen in the presence of excess EDTA may be ascribed to the interaction of EDTA with  $\text{SO}_3^{\cdot-}$ . The residual bisulfite could compete with MB for the generated  $\text{Mn(III)}_{\text{aq}}$  and thus decreased the utilization of  $\text{Mn(III)}_{\text{aq}}$ . In addition, the final pH in the presence of EDTA was always higher than that in the presence of same dosage of PP (Fig. S11). All the evidences suggested that besides serving as a buffer, the inhibition of EDTA on bisulfite consumption and the reducibility of EDTA contributed to its influence on the process of

MB degradation by  $\text{MnO}_2/\text{HSO}_3^-$ . This point was further confirmed by the decomposition of EDTA by  $\text{MnO}_2/\text{HSO}_3^-$  at different initial EDTA concentrations, as shown in Fig. S14. In sum, the influences of ligands on organic contaminant degradation by  $\text{MnO}_2/\text{HSO}_3^-$  are very complex, depending on the properties of ligands.

### 3.4. Influence of co-existing solutes on the degradation kinetics of MB by $\text{MnO}_2/\text{HSO}_3^-$

$\text{Ca}^{2+}$ ,  $\text{Mg}^{2+}$ ,  $\text{HCO}_3^-$ ,  $\text{SO}_4^{2-}$ , and humic acid are frequently present in natural water and thus their influence on the degradation of MB by  $\text{MnO}_2/\text{HSO}_3^-$  was investigated. As presented in Fig. 5, the elevated concentrations of  $\text{Ca}^{2+}$  and  $\text{Mg}^{2+}$  not only accelerated the rate of MB decomposition but also improved the removal efficiencies of MB by  $\text{MnO}_2/\text{HSO}_3^-$ . The dosing of 1.5 mM  $\text{Ca}^{2+}$  and 1.6 mM  $\text{Mg}^{2+}$  shortened the half-lives of MB decomposition from 3.5 s to 1.3 s and 1.6 s, respectively. In the process of MB removal by  $\text{MnO}_2/\text{HSO}_3^-$ , MB was mainly oxidized by  $\text{Mn(III)}_{\text{aq}}$  and the role of  $\text{MnO}_2$  in this process was to react with the negatively charged  $\text{HSO}_3^-$  ions to generate  $\text{Mn(III)}_{\text{aq}}$ . Therefore, in this case, the adsorption of  $\text{Ca}^{2+}$  and  $\text{Mg}^{2+}$  ions, which are positively charged, onto the colloidal  $\text{MnO}_2$  surface would mitigate the negative charge of  $\text{MnO}_2$  and decrease the electrostatic repulsion between  $\text{MnO}_2$  and  $\text{HSO}_3^-$  [52]. Consequently, the reduction of  $\text{MnO}_2$  by  $\text{HSO}_3^-$  was accelerated (as illustrated in Fig. S15) so that  $\text{Mn(III)}_{\text{aq}}$  generation and MB oxidation was enhanced accordingly. The improvement induced by  $\text{Ca}^{2+}$  on MB decomposition by  $\text{MnO}_2/\text{HSO}_3^-$  was more remarkable than that induced by  $\text{Mg}^{2+}$ , which should be associated with the higher affinity of  $\text{Ca}^{2+}$  toward  $\text{MnO}_2$  surface than  $\text{Mg}^{2+}$  [53].

Different from the selected cations, the influence of  $\text{HCO}_3^-$  and  $\text{SO}_4^{2-}$  on the oxidation of MB and the reduction of  $\text{MnO}_2$  was marginal, as demonstrated in Figs. 5 and S13. However, the presence of humic acid exhibited notable negative effect on the elimination of MB by  $\text{MnO}_2/\text{HSO}_3^-$ . The removal of MB dropped from 89.9% to 63.9% and the half-life of MB oxidation was prolonged from 3.5 s to 9.0 s with increasing the concentration of humic acid from 0.0 to 10.0 mg/L, as shown in Fig. 5. The inhibitory effect of humic acid on  $\text{MnO}_2$  reduction was almost comparable to that of  $\text{HCO}_3^-$  and  $\text{SO}_4^{2-}$  (Fig. S15), while it depressed the oxidation of MB to a much greater extent. Thus, the negative effect of humic acid should be mainly associated with its reducibility [14]. It can compete with MB for  $\text{Mn(III)}_{\text{aq}}$  and inhibit the decomposition of MB. Bearing a variety of metal chelating functional groups [14], humic acid might also coordinate with  $\text{Mn(III)}_{\text{aq}}$  and reduce its oxidizing ability toward MB, which deserves further investigation in future.

### 3.5. Oxidation mechanism of organic compounds by $\text{Mn(III)}_{\text{aq}}$

The functional groups of organic contaminants have significant influence on their redox property. The natural charge on the atoms in functional groups is a good parameter related to the reaction mechanisms [54]. Therefore, the DFT calculations were applied to obtain the Mulliken charges of O/N and H in functional groups of ECs and then plotted against the removal of various contaminants in the  $\text{MnO}_2/\text{HSO}_3^-$  process in Fig. 6. As revealed in Fig. 6, the removal of ECs investigated in this study has a quite good negative correlation with the Mulliken charge of O/N or H. The result H, suggesting that the organic contaminants were oxidized by  $\text{Mn(III)}_{\text{aq}}$  via electrophilic attack.

To further explore the mechanisms of organic contaminant degradation in the  $\text{MnO}_2/\text{HSO}_3^-$  process, UPLC-QTOFMS was employed to analyze the degradation intermediates. SMX, one of commonly used antimicrobial agents in treating and preventing diseases in animals, was chosen as a target contaminant in this part. Although different intermediates have been proposed in various degradation processes, the SMX degradation pathway in the  $\text{MnO}_2/\text{HSO}_3^-$  process has not yet been reported.

Twelve transformation products of SMX were identified, as summarized in Table S3, and the chemical structures of these products were proposed on the basis of (i) the structure of SMX, (ii) their precursor ion masses with a high grade of accuracy ( $< 5$  m Da error), (iii) the relative chromatographic retention times, and (iv) previously reported information on the degradation products during various oxidative processes involving SMX. Eight of them (TP1, TP3, TP5, TP6, TP7, TP8, TP10 and TP11) have been proposed in the process of SMX oxidation by electrolysis [55], photolysis [56], photo-Fenton [57], chlorine [58], permanganate [59], ozone [60,61], sulfate radical [62], or ferrate [63], while the other four degradation products have not been previously reported. The major transformation pathways leading to SMX degradation were proposed, as illustrated in Fig. 7, based mainly upon the identified intermediates. Multiple sites could be attacked by  $\text{Mn(III)}_{\text{aq}}$  with different reaction mechanisms. A fraction of SMX was hydrolyzed, with the break of S–N and S–C bonds, to generate TP1, TP5 and TP6, which were also observed in the process of SMX oxidation by  $\text{HO}^\cdot$  [55],  $\text{O}_2^{\cdot-}$  [64] and ozone [59]. Further oxidation of these hydrolysates (TP5 and TP6) was evidenced by the cleavage of the isoxazole ring. The formation of TP11 could be attributed to the oxidation of the methyl group on the isoxazole ring to yield a carboxylic acid group, analogous to the degradation mechanism of SMX by ozone [59]. Subsequent hydrolytic reaction of S–N bond and cleavage of benzene and isoxazole ring resulted in the generation of TP3 and TP12. The addition reaction of  $\text{H}_2\text{O}$  with carbon-carbon double bonds on the isoxazole ring transformed SMX to TP9, followed by further oxidation to TP12. The addition of –OH substituent to the benzene ring could improve the oxidation of SMX by  $\text{Mn(III)}_{\text{aq}}$  since the phenolic hydroxyl was an electron-donating group, which facilitated the subsequent degradation of TP8 [59]. The amino group, an electron-rich group [65], is vulnerable to attack by  $\text{Mn(III)}_{\text{aq}}$ , accounting for the generation of TP7 [66]. Therefore, the degradation pathways of SMX in the  $\text{MnO}_2/\text{HSO}_3^-$  process were consistent with the DFT calculation results, which showed that organic contaminants were oxidized by  $\text{Mn(III)}_{\text{aq}}$  via electrophilic attack.

Measurements of total organic carbon (TOC) at the end of SMX in  $\text{MnO}_2/\text{HSO}_3^-$  process oxidation showed limited mineralization (Fig. S16), which might be ascribed to the short lifetime of  $\text{Mn(III)}_{\text{aq}}$ . To achieve high mineralization of the contaminants, continuous generation of  $\text{Mn(III)}_{\text{aq}}$  should be considered, which will be verified in future.

## 4. Conclusions

The  $\text{MnO}_2/\text{HSO}_3^-$  process degraded contaminants with diverse organic moieties more quickly and effectively than  $\text{MnO}_2$  alone. Various results showed that  $\text{Mn(III)}_{\text{aq}}$ , the electrophilic oxidant, was the reactive oxidant in  $\text{MnO}_2/\text{HSO}_3^-$  process. The kinetics of MB degradation were affected by complexing ligands and co-existing solutes. The  $\text{Mn(III)}_{\text{aq}}$  intermediate induces fast degradation of organic contaminants, which should be considered in environmental fate models to better evaluate the fate of organic pollutants in environment. The results of this study reveal that the  $\text{MnO}_2/\text{HSO}_3^-$  process can alleviate the challenges in  $\text{MnO}_2$  application and is a promising one for decomposing organic contaminants in water and wastewater under acidic conditions. Moreover, the mixture of  $\text{MnO}_2$  coated sand and  $\text{CaSO}_3$ , a slow-releasing  $\text{SO}_3^{2-}$  source, may work as the media in stormwater infiltration system for destructing organic contaminants in acid rain.

## Acknowledgements

This work was supported by the National Natural Science Foundation of China (Grant 21522704), the State Key Laboratory of Pollution Control and Resource Reuse Foundation (No. PCRRK16001), and the Initiation Grant of HKUST (No. IGN17EG07).

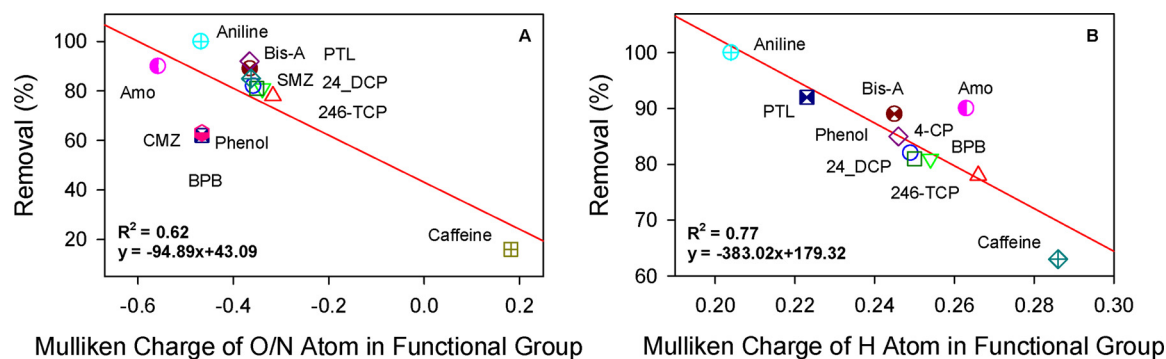


Fig. 6. Correlations between the removal efficiency of EPs obtained after 10 s in  $\text{MnO}_2/\text{HSO}_3^-$  process and the Mulliken charge of (A) O/N atom in functional group, (B) H atom in functional group.

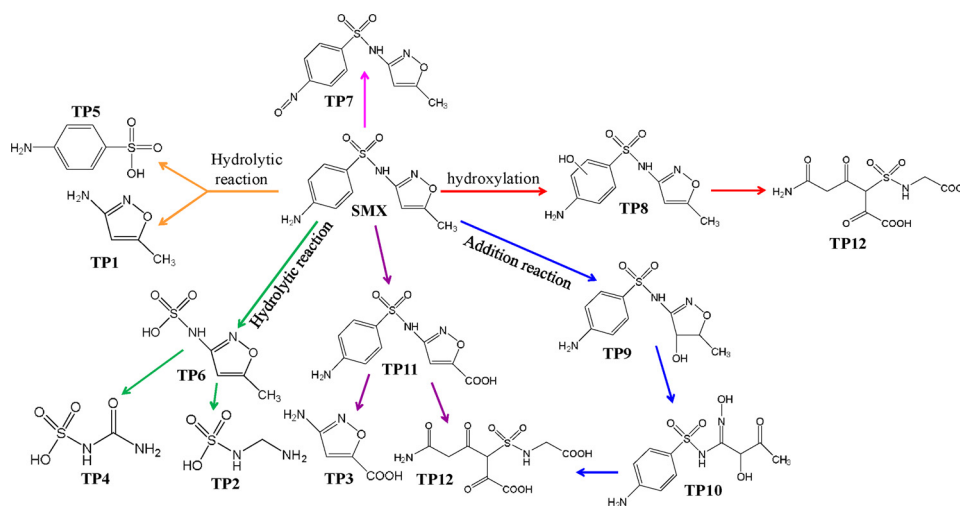


Fig. 7. Proposed degradation pathways of SMX in the  $\text{MnO}_2/\text{HSO}_3^-$  process.

## Appendix A. Supplementary data

Supplementary material related to this article can be found, in the online version, at doi:<https://doi.org/10.1016/j.jhazmat.2018.10.002>.

## References

- [1] C.N. Butterfield, A.V. Soldatova, S.W. Lee, T.G. Spiro, B.M. Tebo, Mn(II,III) oxidation and  $\text{MnO}_2$  mineralization by an expressed bacterial multicopper oxidase, *Proc. Natl. Acad. Sci. U.S.A.* 110 (2013) 11731–11735.
- [2] A.S. Madison, B.M. Tebo, A. Mucci, B. Sundby, G.W. Luther III, Abundant porewater Mn(III) is a major component of the sedimentary redox system, *Science* 341 (2013) 875–878.
- [3] K.S. Johnson, Manganese redox chemistry revisited, *Science* 313 (2006) 1896–1897.
- [4] J.E. Kostka, G.W. Luther III, K.H. Nealson, Chemical and biological reduction of Mn(III)-pyrophosphate complexes: potential importance of dissolved Mn(III) as an environmental oxidant, *Geochim. Cosmochim. Acta* 59 (1995) 885–894.
- [5] B.M. Tebo, Manganese(II) oxidation in the suboxic zone of the Black Sea, *Deep-Sea Res. PT I* (38 Suppl.) (1991) S883–S905 2.
- [6] R.E. Trouwborst, B.G. Clement, B.M. Tebo, B.T. Glazer, L.G. Rd, Soluble Mn(III) in suboxic zones, *Science* 313 (2006) 1955–1957.
- [7] Z.M. Wang, W. Xiong, B.M. Tebo, D.E. Giammar, Oxidative  $\text{UO}_2$  dissolution induced by soluble Mn(III), *Environ. Sci. Technol.* 48 (2014) 289–298.
- [8] C.K. Remucal, M. Ginder-Vogel, A critical review of the reactivity of manganese oxides with organic contaminants, *Environ. Sci. Proc. Impacts* 16 (2014) 1247–1266.
- [9] M. Zhu, M. Ginder-Vogel, S.J. Parikh, X.H. Feng, D.L. Sparks, Cation effects on the layer structure of biogenic Mn-oxides, *Environ. Sci. Technol.* 44 (2010) 4465–4471.
- [10] H.L. Cui, X.W. Liu, W.F. Tan, H.D. Ruan, Influence of Mn(III) availability on the phase transformation from layered buserite to tunnel-structured todorokite, *Clay Clays Miner.* 56 (2008) 397–403.
- [11] J. Klausen, S.B. Haderlein, R.P. Schwarzenbach, Oxidation of substituted anilines by aqueous  $\text{MnO}_2$ : effect of co-solutes on initial and quasi-steady-state kinetics, *Environ. Sci. Technol.* 31 (1997) 2642–2649.
- [12] S. Laha, R.G. Luthy, Oxidation of aniline and other primary aromatic amines by manganese dioxide, *Environ. Sci. Technol.* 24 (1990) 363–373.
- [13] H. Li, L.D. Lee, C.T. Jafvert, J.G. Gravelle, Effect of substitution on irreversible binding and transformation of aromatic amines with soils in aqueous systems, *Environ. Sci. Technol.* 34 (2000) 3674–3680.
- [14] B. Sun, J. Zhang, J.S. Du, J.L. Qiao, X.H. Guan, Reinvestigation of the role of humic acid in the oxidation of phenols by permanganate, *Environ. Sci. Technol.* 47 (2013) 14332–14340.
- [15] L. Xu, C. Xu, M.R. Zhao, Y.P. Qiu, G.D. Sheng, Oxidative removal of aqueous steroid estrogens by manganese oxides, *Water Res.* 42 (2008) 5038–5044.
- [16] H. Zhang, C.H. Huang, Oxidative transformation of triclosan and chlorophene by manganese oxides, *Environ. Sci. Technol.* 37 (2003) 2421–2430.
- [17] K.A. Barrett, M.B. McBride, Oxidative degradation of glyphosate and aminomethylphosphonate by manganese oxide, *Environ. Sci. Technol.* 39 (2005) 9223–9228.
- [18] X. Yang, C. Shang, Chlorination byproduct formation in the presence of humic acid, model nitrogenous organic compounds, ammonia, and bromide, *Environ. Sci. Technol.* 38 (2004) 4995–5001.
- [19] B. Sun, D.D. Rao, Y.H. Sun, X.H. Guan, Auto-accelerating and auto-inhibiting phenomena in the oxidation process of organic contaminants by permanganate and manganese dioxide under acidic conditions: effects of manganese intermediates/products, *RSC Adv.* 6 (2016) 62858–62865.
- [20] B. Sun, X.H. Guan, J.Y. Fang, P.G. Tratnyek, Activation of manganese oxidants with bisulfite for enhanced oxidation of organic contaminants: the involvement of Mn(III), *Environ. Sci. Technol.* 49 (2015) 12414–12421.
- [21] D.J. Lapworth, N. Baran, M.E. Stuart, K. Manamsa, J. Talbot, Persistent and emerging micro-organic contaminants in Chalk groundwater of England and France, *Environ. Pollut.* 203 (2015) 214–225.
- [22] B. Petrie, R. Barden, B. Kasprzyk-Hordern, A review on emerging contaminants in wastewaters and the environment: current knowledge, understudied areas and recommendations for future monitoring, *Water Res.* 72 (2015) 3–27.
- [23] J. Zhang, B. Sun, X.M. Xiong, N.Y. Gao, W.H. Song, E.D. Du, X.H. Guan, G.M. Zhou, Removal of emerging pollutants by  $\text{Ru}/\text{TiO}_2$ -catalyzed permanganate oxidation, *Water Res.* 63 (2014) 262–270.
- [24] R.E. Humphrey, M.H. Ward, W. Hinze, Spectrophotometric determination of sulfite with 4,4'-dithio-dipyridine and 5,5'-dithiobis (2-nitrobenzoic acid), *Anal. Chem.* 42 (1970) 698–702.
- [25] J. Tomasi, B. Mennucci, R. Cammi, Quantum mechanical continuum solvation models, *Chem. Rev.* 105 (2005) 2999–3093.

- [26] R.S. Mulliken, Electronic population analysis on LCAO-MO molecular wave functions. I, *J. Phys. Chem.* 23 (1955) 1833–1840.
- [27] K.D. Lin, W.P. Liu, J. Gan, Oxidative removal of bisphenol A by manganese dioxide: efficacy, products, and pathways, *Environ. Sci. Technol.* 43 (2009) 3860–3864.
- [28] S.D. Richardson, Environmental mass spectrometry: emerging contaminants and current issues, *Anal. Chem.* 78 (2006) 4021–4046.
- [29] B. Sun, H.Y. Dong, D. He, D.D. Rao, X.H. Guan, Modeling the kinetics of contaminants oxidation and the generation of manganese(III) in the permanganate/bisulfite process, *Environ. Sci. Technol.* 50 (2016) 1473–1482.
- [30] H.Y. Dong, G.F. Wei, W.J. Fan, S.C. Ma, H.Y. Zhao, W.X. Zhang, X.H. Guan, T.J. Strathmann, Reinvestigating the role of reactive species in the oxidation of organic co-contaminants during Cr(VI) reactions with sulfite, *Chemosphere* 196 (2018) 593.
- [31] S.F. Sun, S.Y. Pang, J. Jiang, J. Ma, Z.S. Huang, J.M. Zhang, Y.L. Liu, C.B. Xu, Q.L. Liu, Y.X. Yuan, The combination of ferrate(VI) and sulfite as a novel advanced oxidation process for enhanced degradation of organic contaminants, *Chem. Eng. J.* 333 (2017) 11–19.
- [32] L. Chen, M. Tang, C. Chen, M. Chen, K. Luo, J. Xu, D. Zhou, F. Wu, Efficient bacterial inactivation by transition metal catalyzed auto-oxidation of sulfite, *Environ. Sci. Technol.* 51 (2017) 12663–12671.
- [33] L. Chen, X.Z. Peng, J.H. Liu, J.J. Li, F. Wu, Decolorization of orange II in aqueous solution by an Fe(II)/sulfite system: replacement of persulfate, *Ind. Eng. Chem. Res.* 51 (2012) 13632–13638.
- [34] G.V. Buxton, C.L. Greenstock, W.P. Helman, A.B. Ross, Critical review of rate constants for reactions of hydrated electrons, hydrogen atoms and hydroxyl radicals ( $\cdot\text{OH}/\cdot\text{O}^-$ ) in aqueous solution, *J. Phys. Chem. Ref. Data* 17 (1988) 513–886.
- [35] M.M. Huber, S. Canonica, G.Y. Park, U. Von Gunten, Oxidation of pharmaceuticals during ozonation and advanced oxidation processes, *Environ. Sci. Technol.* 37 (2003) 1016–1024.
- [36] P. Neta, R.E. Huie, A.B. Ross, Rate constants for reactions of inorganic radicals in aqueous solution, *J. Phys. Chem. Ref. Data* 17 (1988) 1027–1284.
- [37] P. Neta, V. Madhavan, H. Zemel, R.W. Fessenden, Rate constants and mechanism of reaction of sulfate radical anion with aromatic compounds, *Chem. Inform.* 8 (1977) 163–164.
- [38] R. Matta, S. Tlili, S. Chiron, S. Barbati, Removal of carbamazepine from urban wastewater by sulfate radical oxidation, *Environ. Chem. Lett.* 9 (2011) 347–353.
- [39] A. Monod, A. Chebbi, R. Durand-Jolibois, P. Carlier, Oxidation of methanol by hydroxyl radicals in aqueous solution under simulated cloud droplet conditions, *Atmos. Environ.* 34 (2000) 5283–5294.
- [40] C.R. Keenan, D.L. Sedlak, Factors affecting the yield of oxidants from the reaction of nanoparticulate zero-valent iron and oxygen, *Environ. Sci. Technol.* 42 (2008) 1262–1267.
- [41] P.D. Bartlett, J.D. Cotman, The kinetics of the decomposition of potassium persulfate in aqueous solutions of methanol, *J. Am. Chem. Soc.* 71 (1949) 1419–1422.
- [42] J. Zhang, J. Ma, H. Song, S. Sun, Z. Zhang, T. Yang, Organic contaminants degradation from the S(IV) autoxidation process catalyzed by ferrous-manganous ions: a noticeable Mn(III) oxidation process, *Water Res.* 133 (2018) 227–235.
- [43] S.M. Webb, G.J. Dick, J.R. Bargar, B.M. Tebo, Evidence for the presence of Mn(III) intermediates in the bacterial oxidation of Mn(II), *Proc. Natl. Acad. Sci. U. S. A.* 102 (2005) 5558–5563.
- [44] B. Sun, Q.Q. Bao, X.H. Guan, Critical role of oxygen for rapid degradation of organic contaminants in permanganate/bisulfite process, *J. Hazard. Mater.* 352 (2018) 157–164.
- [45] P.S. Nico, R.J. Zasoski, Importance of Mn(III) availability on the rate of Cr(III) oxidation on  $\delta\text{-MnO}_2$ , *Environ. Sci. Technol.* 34 (2000) 3363–3367.
- [46] P.S. Nico, R.J. Zasoski, Mn(III) center availability as a rate controlling factor in the oxidation of phenol and sulfide on  $\delta\text{-MnO}_2$ , *Environ. Sci. Technol.* 35 (2001) 3338–3343.
- [47] J.K. Klewicki, J.J. Morgan, Kinetic behavior of Mn(III) complexes of pyrophosphate, EDTA, and citrate, *Environ. Sci. Technol.* 32 (1998) 2916–2922.
- [48] V. Marinović, A.R. Despić, Pyrophosphoric acid as a source of hydrogen in cathodic hydrogen evolution on silver, *Electrochim. Acta* 44 (1999) 4073–4077.
- [49] H. Sun, M.Z. Hoffman, Reductive quenching of the excited states of ruthenium(II) complexes containing 2,2'-Bipyridine, 2,2'-Bipyrazine, and 2,2'-Bipyrimidine Ligands, *J. Phys. Chem.* 98 (1994) 11719–11726.
- [50] G. Davies, Some aspects of the chemistry of manganese(III) in aqueous solution, *Coord. Chem. Rev.* 4 (1969) 199–224.
- [51] L.D. Wang, Y.L. Ma, J.M. Hao, Y. Zhao, Mechanism and kinetics of sulfite oxidation in the presence of ethanol, *Ind. Eng. Chem. Res.* 48 (2009) 4307–4311.
- [52] R.P. Liu, H.J. Liu, Z.M. Qiang, J.H. Qu, G.B. Li, D.S. Wang, Effects of calcium ions on surface characteristics and adsorptive properties of hydrous manganese dioxide, *J. Colloid Interface Sci.* 331 (2009) 275–280.
- [53] H.S. Posselt, F.J. Anderson, W.J. Weber, Cation sorption on colloidal hydrous manganese dioxide, *Environ. Sci. Technol.* 2 (1968) 1087–1093.
- [54] J.S. Du, B. Sun, J. Zhang, X.H. Guan, Parabola-like shaped pH-rate profile for phenols oxidation by aqueous permanganate, *Environ. Sci. Technol.* 46 (2012) 8860–8867.
- [55] H. Lin, J.F. Niu, J.L. Xu, Y. Li, Y.H. Pan, Electrochemical mineralization of sulfamethoxazole by Ti/SnO<sub>2</sub>-Sb/Ce-PbO<sub>2</sub> anode: kinetics, reaction pathways, and energy cost evolution, *Electrochim. Acta* 97 (2013) 167–174.
- [56] L.H. Hu, P.M. Flanders, P.L. Miller, T.J. Strathmann, Oxidation of sulfamethoxazole and related antimicrobial agents by TiO<sub>2</sub> photocatalysis, *Water Res.* 41 (2007) 2612–2626.
- [57] A.G. Trovó, R.F.P. Nogueira, A. Ana, A.R. Fernandez-Alba, S. Carla, M. Sixto, Degradation of sulfamethoxazole in water by solar photo-Fenton. Chemical and toxicological evaluation, *Water Res.* 43 (2009) 3922–3931.
- [58] M.C. Dodd, C.H. Huang, Transformation of the antibacterial agent sulfamethoxazole in reactions with chlorine: kinetics, mechanisms, and pathways, *Environ. Sci. Technol.* 38 (2004) 5607–5615.
- [59] S.S. Gao, Z.W. Zhao, Y.P. Xu, J.Y. Tian, Q. Hong, L. Wei, F.Y. Cui, Oxidation of sulfamethoxazole (SMX) by chlorine, ozone and permanganate—a comparative study, *J. Hazard. Mater.* 274 (2014) 258–269.
- [60] M.D.M. Gómez-Ramos, M. Mezcuca, A. Agüera, A.R. Fernández-Alba, S. Gonzalo, A. Rodríguez, R. Rosal, Chemical and toxicological evolution of the antibiotic sulfamethoxazole under ozone treatment in water solution, *J. Hazard. Mater.* 192 (2011) 18–25.
- [61] Y.H. Ren, C.B. Du, S.J. Feng, C.L. Wang, Z.P. Kong, B. Yue, H.Y. He, Three POM-based coordination polymers: hydrothermal synthesis, characterization, and catalytic activity in epoxidation of styrene, *Crystengcomm* 13 (2011) 7143–7148.
- [62] M.M. Ahmed, S. Barbati, P. Doumenq, S. Chiron, Sulfate radical anion oxidation of diclofenac and sulfamethoxazole for water decontamination, *Chem. Eng. J.* 197 (2012) 440–447.
- [63] V.K. Sharma, S.K. Mishra, N. Nesnas, Oxidation of sulfonamide antimicrobials by ferrate(VI), *Environ. Sci. Technol.* 40 (2007) 7222–7227.
- [64] S.Y. Ding, J.F. Niu, Y.P. Bao, L.J. Hu, Evidence of superoxide radical contribution to demineralization of sulfamethoxazole by visible-light-driven Bi<sub>2</sub>O<sub>3</sub>/Bi<sub>2</sub>O<sub>2</sub>CO<sub>3</sub>/Sr<sub>6</sub>Bi<sub>2</sub>O<sub>9</sub> photocatalyst, *J. Hazard. Mater.* 262 (2013) 812–818.
- [65] W.Q. Guo, R.L. Yin, X.J. Zhou, J.S. Du, H.O. Cao, S.S. Yang, N.Q. Ren, Sulfamethoxazole degradation by ultrasound/ozone oxidation process in water: kinetics, mechanisms, and pathways, *Ultrason. Sonochem.* 22 (2015) 182–187.
- [66] C.D. Qi, X.T. Liu, C.Y. Lin, X.H. Zhang, J. Ma, H.B. Tan, W. Ye, Degradation of sulfamethoxazole by microwave-activated persulfate: kinetics, mechanism and acute toxicity, *Chem. Eng. J.* 249 (2014) 6–14.